Central Fibroblast Growth Factor 21 Browns White Fat via Sympathetic Action in Male Mice

Nicholas Douris, Darko M. Stevanovic, ffolliott M. Fisher, Theodore I. Cisu, Melissa J. Chee, Ngoc L. Nguyen, Eleen Zarebidaki, Andrew C. Adams, Alexei Kharitonenkov, Jeffrey S. Flier, Timothy J. Bartness, and Eleftheria Maratos-Flier

Division of Endocrinology (N.D., D.M.S., f.M.F., T.I.C., M.J.C., J.S.F., E.M.-F.), Beth Israel Deaconess Medical Center, Department of Medicine, Harvard Medical School, Boston, Massachusetts 02215-5491; Institute of Medical Physiology (D.M.S.), School of Medicine, University of Belgrade, 11000 Belgrade, Serbia; Department of Biology and Center for Obesity Reversal (N.L.N., E.Z., T.J.B.), Georgia State University, Atlanta, Georgia 30302-4010; and Diabetes Research (A.C.A., A.K.), Lilly Research Laboratories, Lilly Corporate Center, Indianapolis, Indiana 46285-0001

Fibroblast growth factor 21 (FGF21) has multiple metabolic actions, including the induction of browning in white adipose tissue. Although FGF21 stimulated browning results from a direct interaction between FGF21 and the adipocyte, browning is typically associated with activation of the sympathetic nervous system through cold exposure. We tested the hypothesis that FGF21 can act via the brain, to increase sympathetic activity and induce browning, independent of cell-autonomous actions. We administered FGF21 into the central nervous system via lateral ventricle infusion into male mice and found that the central treatment increased norepinephrine turnover in target tissues that include the inguinal white adipose tissue and brown adipose tissue. Central FGF21 stimulated browning as assessed by histology, expression of uncoupling protein 1, and the induction of gene expression associated with browning. These effects were markedly attenuated when mice were treated with a β-blocker. Additionally, neither centrally nor peripherally administered FGF21 initiated browning in mice lacking β-adrenoceptors, demonstrating that an intact adrenergic system is necessary for FGF21 action. These data indicate that FGF21 can signal in the brain to activate the sympathetic nervous system and induce adipose tissue thermogenesis. (**Endocrinology** 156: 2470–2481, 2015)

Fibroblast growth factor 21 (FGF21), an endocrine member of the FGF superfamily, is an important regulator of energy homeostasis, particularly in response to nutritional challenges such as fasting, consumption of a ketogenic diet (KD), or amino acid restriction such as methionine or leucine-deficient diets (1–4). FGF21 acts through several known FGF receptors: Fgfr1c, Fgfr2c, and Fgfr3c as well as the obligate coreceptor, β-klotho (5–10).

Systemic pharmacological effects include the lowering of circulating glucose, triglycerides and improved insulin sensitivity. In addition, overexpression and systemic treatment with FGF21 increase energy expenditure and protect against diet-induced obesity (11, 12).

FGF21 and thermoregulation have been linked as FGF21 activates brown adipose tissue (BAT) and induces browning of white adipose tissue (WAT) (13–16). Brown-

Abbreviations: ABC, avidin-biotin complex; aCSF, artificial CSF; AMPT, α-methyl-p-tyrosine; BAT, brown adipose tissue; C/ebp, CCAAT/enhancer-binding protein; CNS, central nervous system; Cox, cytochrome c oxidase polypeptide; CSF, cerebrospinal fluid; Dio2, deiodinase 2; EWAT, epididymal WAT; Fgfr, Fibroblast growth factor receptor; FGF21, fibroblast growth factor 21; h, human; IBAT, interscapular BAT; icv, intracerebroventricular; IML, intermediolateral nucleus; IWAT, inguinal WAT; KD, ketogenic diet; Lcad, long-chain acyl-coenzyme A dehydrogenase; NE, norepinephrine; NETO, NE turnover; p-Erk, phosphorylated Erk 1/2; Pgc-1α, coactivator 1 α; Ppar, peroxisome proliferator-activated receptor; PVH, paraventricular hypothalamus; RT, room temperature; SNS, sympathetic nervous system; SVF, stromal-vascular fraction; Ucp1, uncoupling protein 1; Vlcad, very-Lcad; VO$_2$, volume oxygen consumption; WAT, white adipose tissue; WT, wild type; ZT, zeitgeber time.

ing, an adaptive response typically seen with chronic cold exposure, increases thermogenic capacity by converting WAT to a brown-like state. Hallmarks of browning include the appearance of uncoupling protein 1 (UCP1)-expressing mitochondrial-rich multilocular adipocytes in WAT, otherwise known as "brite" (brown-in-white) or "beige" adipocytes. These brite cells are highly metabolically active (17), and many genetic mutations leading to a lean phenotype also are associated with browning of WAT (18, 19). Furthermore, cold exposure and β-adrenoceptor stimulation induce FGF21 gene expression in BAT as well as in fat depots susceptible to browning, including inguinal WAT (IWAT) and perirenal adipose tissue (13, 14, 20, 21). By contrast, mice lacking FGF21 have an attenuated response to cold, including impaired formation of brite cells (13). In aggregate, these data suggest that FGF21 is an intrinsic mediator of the response to cold.

The thermogenic effects of FGF21 on adipocytes are cell-autonomous. Direct actions of FGF21 enhance peroxisome proliferator-activated receptor (PPAR)γ, coactivator 1 α (PGC-1α) protein levels independent of transcription (13). During cold exposure, the sympathetic nervous system (SNS) also plays a major role to increase sympathetic activity in the periphery, ultimately resulting in increased activation of β-adrenoceptors in WAT and BAT. This activation includes multiple relays from a distributed network across the neuroaxis and integrated, in part through the paraventricular hypothalamus (PVH) to the intermediolateral nucleus (IML), and sympathetic ganglia synapsing in adipose tissue (22). Thus, beyond the described cell-autonomous effects of FGF21 in browning, we examined whether FGF21 may also act through a centrally mediated pathway via the SNS to control metabolism.

FGF21 crosses the blood brain barrier in mice (23) and is found in cerebrospinal fluid (CSF) in humans (24). Indeed, the FGF21 signaling system is present in the brain and includes receptors Fgfr1 receptors as well as the coreceptor β-klotho (25–28). In addition, consistent with central action one study reported that intracerebroventricularly (icv) administered FGF21 in an obese rat model improved glucose homeostasis and increased energy expenditure (29). Subsequent reports indicated that FGF21 can act on the hypothalamus and hindbrain to induce a "starvation state." This included reduced growth, lowered insulin, increased corticosterone, altered behavioral activity rhythms and inhibition of female fertility by suppressing vasopressin-kisspeptin signaling and thereby inhibiting LH (25, 26). The model utilized in those studies, overexpresses FGF21 at supraphysiologic levels, making it difficult to distinguish the primary effects on the brain vs the periphery.

We now show that FGF21 can act in the brain to increase sympathetic activity. The resulting increase in adrenergic signaling leads to increased norepinephrine (NE) turnover in fat depots, associated browning of IWAT and activation of BAT. β-Adrenergic antagonism blocks the actions of central FGF21 but only has a partial effect on peripherally administered FGF21. Mice lacking all 3 β-adrenoceptors show no thermogenic response to FGF21. Thus, we show that a primary and direct effect of FGF21 in the brain is to activate the SNS for thermogenic adaptation.

Materials and Methods

Animals

All experiments were carried out on male wild-type (WT) C57Bl/6 mice or male mice homozygous for disruption of β1, β2, and β3 adrenoceptors used in the genetic sympathectomy studies (30). Genotypes of parental strains in The Jackson Laboratory nomenclature are Ardb1, 2tm1Bkk (β 1,2 knockout), and Ardb3tm1Lowl (β 3 knockout). Male mice were individually housed and provided with ad libitum access to water and rodent chow LabDiet 5008 (Pharmaserv) and under a 12-hour light, 12-hour dark cycle and an ambient temperature of 22 ± 2°C. At the start of the experiment, mice were approximately 14 weeks old. All procedures were in accordance with National Institutes of Health Guidelines for the Care and Use of Animals and were approved by the Institutional Animal Care and Use Committee.

Animal measurements

Indirect calorimetry

Mice were maintained on a 12-hour light, 12-hour dark cycle and metabolic rate was measured by indirect calorimetry using a Comprehensive Lab Animal Monitoring System (Columbus Instruments). Sample air was passed through an O_2 sensor (Columbus Instruments) for determination of O_2 content. O_2 consumption was calculated by examining the difference of O_2 concentration of air entering the chamber compared with air leaving the chamber. The sensor was calibrated against a standard gas mix containing defined quantities of O_2, CO_2, and nitrogen. Food and water were available ad libitum. Mice were measured for 24 hours of data collection, which were averaged and binned to create day and night depictions of metabolic rate and normalized to effective mass ($(VO_2/mass^{\wedge}(2/3))$).

Feeding and weight collection

Mice were maintained on a 12-hour light, 12-hour dark cycle on a standard chow diet LabDiet 5008 (Pharmaserv). Food intake and body weights were determined with a tabletop scale measured to the closest 0.1 g.

Home cage activity

Spontaneous locomotor activity was recorded continuously using the OptoM3 apparatus beam breaks from Columbus Instruments.

Table 1.   Circulating Metabolic Parameters of Mouse Cohorts Administered icv-FGF21 or sc-FGF21

Serum Concentrations	0.4-μg/d icv-FGF21			1.6-μg/d sc-FGF21		
	Vehicle	Treated	P Value	Vehicle	Treated	P Value
β-Hydroxybutyrate (mM)	0.16 ± 0.01	0.17 ± 0.01	ns	0.15 ± 0.01	0.16 ± 0.02	ns
Glucose (mg/dL)	179 ± 7	182 ± 7	ns	183 ± 9	204 ± 18	ns
Triglycerides (mg/dL)	82 ± 9	67 ± 6	ns	76 ± 10	64 ± 5	ns

Serum analysis

Both mouse and human serum FGF21 concentrations were measured according to the manufacturer's instructions using quantitative ELISAs specific for mouse or human FGF21 (R&D Systems).

Quantitative RT-PCR

RNA was isolated from tissue flash-frozen in liquid nitrogen using an RNAeasy mini kit (QIAGEN) according to manufacturer's instructions. A deoxyribonuclease (QIAGEN) step to digest the genomic DNA was included. cDNA was made from isolated RNA using oligo(dt) and random hexamer primers and reverse transcriptase (QuantiTech RT kit; QIAGEN). Quantitative PCR was performed using the 7800HT (Applied Biosystems) thermal cycler and SYBR Green master mix (Applied Biosystems). Relative mRNA abundance was calculated and normalized to levels of TATA box-binding protein. Primers are included in Table 2.

Recombinant FGF21 protein

In brief, human FGF21 (hFGF21) was expressed in *Escherichia coli* and was subsequently refolded in vitro and isolated as previously described (11).

Central FGF21 infusion

Each mouse was anesthetized with ketamine/xylazine and the surgical area shaved and cleaned with an iodine solution and alcohol swab. After being placed into a stereotaxic frame, an incision running dorsally and laterally of 1.5 cm was made to expose the skull, which was cleaned and drilled at the next coordinates for the third ventricle: anterioposterior, −0.5 mm and lateral, ±1 mm from the bregma. The cannula (Plastics One) was then implanted at a cut −2.5 mm below the dura. The cannula

was secured with cyanoacrylate adhesive Loctite 454 (Durect Corp). Subsequently, an Alzet osmotic minipump (Alzet model 1007D; Durect Corp) filled with saline vehicle or hFGF21 (E. Lilly), was implanted by insertion under the skin between the scapulae and connected to the cannula via vinyl catheter tubing (Durect Corp) and sutures were used to close the wound. The pumps were loaded to deliver 0.4 μg/12 μL/d of hFGF21 or 12 μL/d of saline vehicle alone.

Peripheral FGF21 infusion

Mice were anesthetized with isoflurane, and an Alzet osmotic minipump (Alzet model 1007D; Durect Corp) filled with saline or hFGF21 (E. Lilly), was implanted sc by insertion under the skin between the scapulae. Sutures were used to close the wound. The pumps were loaded to deliver doses of hFGF21 or saline vehicle as indicated in the main text.

β-Adrenoceptor antagonism

Mice were given daily ip injections with ((s)-(-) propranolol hydrochloride; Sigma) at 5 mg/kg·d for 5 days before icv surgery. Upon surgery, propranolol was included in the same Alzet miniosmotic pump that introduced hFGF21 or saline vehicle at the same 5-mg/kg·d dose.

In vitro hypothalamic slice culture

Slices were prepared as previously described (31, 32). Briefly, brains from 10-week-old male C57BL/6 mice were rapidly removed and submerged in ice-cold carbogenated (95% O_2/5% CO_2) artificial CSF (aCSF) containing: 124mM NaCl, 3mM KCl, 1.3mM $MgSO_4$, 1.4mM NaH_2PO_4, 10mM glucose, 26mM $NaHCO_3$, 2.5mM $CaCl_2$, and 5mM 3-(N-morpholino)propanesulfonic acid (300–302 mOsm/L). Coronal sections (250 μm) containing the PVH were cut from a brain block using a vi-

Table 2.   List of Primers

Gene	F	R
β-Klotho	CGAGCCCATTGTTACCTTGT	CATGCATACCTGTGCCAAAC
C/ebpβ	GCAAGAGCCGCGACAAG	GGCTCGGGCAGCTGCTT
Cox7α	AAAACCGTGTGGCAGAGAAG	CCAGCCCAAGCAGTATAAGC
Cox8β	TGCGAAGTTCACAGTGGTTC	TGCTGCGGAGCTCTTTTTAT
Cpt1β	GTCGCTTCTTCAAGGTCTGG	AAGAAAGCAGCACGTTCGAT
Dio2	GTGGCTGACTTCCTGTTGGT	GCACACACGTTCAAAGGCTA
Fgfr1	TGTTTGACCGGATCTACACACA	CTCCCACAAGAGCACTCCAA
Fgf21	CTGGGGGTCTACCAAGCATA	CACCCAGGATTTGAATGACC
Lcad	TCTTTTCCTCGGAGCATGACA	GACCTCTCTACTCACTTCTCCAG
Pgc-1α	CCCTGCCATTGTTAAGACC	TGCTGCTGTTCCTGTTTTC
Tbp	AATGACTCACAAGGCAATGTCG	AGCTTTTCTAGCCCGTTTCAAT
Ucp1	ACTGCCACACCTCCAGTCATT	CTTTGCCTCACTCAGGATTGG
Vlcad	TATCTCTGCCCAGCGACTTT	TGGGTATGGGAACACCTGAT

Forward primer (F) and reverse primer (R) used for amplification using QRT-PCR. *Tbp*, TATA box-binding protein.

Table 3. Antibody Table

Peptide/ Protein Target	Antigen Sequence (if known)	Name of Antibody	Manufacturer, Catalog Number, and/or Name of Individual Providing the Antibody	Species Raised in; Monoclonal or Polyclonal	Dilution Used
p-Erk	Phospho-p44/42 MAPK (ERK 1/2), Thr 202/Tyr204		Cell Signaling, catalog 4370	Rabbit; monoclonal	1:1000
		AffiniPure goat antirabbit Biotin-SP-conjugated secondary	Jackson ImmunoResearch, catalog 111-035-144	Goat	1:1000 for p-Erk, 1:200 for Ucp1
Ucp1		Anti-Ucp1	Abcam, catalog 10983	Rabbit; polyclonal	1:500

bratome (Leica VT100S). Slices were held in holding chamber containing carbogenated aCSF at room temperature (RT) for 2–3 hours, then equilibrated in experimental chambers at 34°C for 1.5 hours. This prewarmed chamber was spiked with 100nM hFGF21 where slices were incubated for 10 minutes. Control brain slices were kept in aCSF bath (34°C) and did not receive further treatment. After the application period, all slices were placed in 10% formalin (24 h, 4°C), cryoprotected with 20% sucrose (24 h, 4°C), and resectioned to 50-μm thickness using a freezing microtome (Leica SM2000R). Control and FGF21-treated slices were processed for phosphorylated ERK (p-Erk) immunohistochemistry.

Acute in vivo brain signaling

Because exogenous treatment with FGF21 leads to an induction of MAPK signaling cascade, phosphorylation of Erk1/2 was used as an indicator of FGF21 activity. In brief, mice were injected with 24-μg FGF21/mouse ip and perfused with 10% formalin 30 minutes later. Postfixation of brains was performed with 10% formalin (24 h, 4°C), cryoprotected with 20% sucrose (24 h, 4°C), and sectioned to 30-μm thickness using a freezing microtome (Leica SM2000R). Brains were then processed for p-Erk immunohistochemistry.

Immunohistochemistry

Immunohistochemical staining of Ucp1-positive IWAT

WAT was dissected and fixed in 4% formaldehyde, embedded in paraffin, and cut into 6-μm sections. Each slide was incubated with anti-Ucp1 antibody and the signal developed, by: 1) antigen retrieval with citric acid and 3% hydrogen peroxide; 2) 10% normal goat serum for 30 minutes; 3) incubation with anti-Ucp1 antibody for 30 minutes at 37°C; 4) biotinylated IgG secondary antibody for 90 minutes at 37°C; 5) avidin-biotin complex (ABC) kit, as per manufacturer's instructions (Vector Laboratories); and 6) developed signal with 3, 3'-diaminobenzidine substrate (Vector Laboratories) and subsequent rapid hemotoxylin counterstain. Slides were mounted after dehydrating through ethanol and cleared with xylene.

Immunohistochemical staining of p-Erk1/2

Serial coronal free-floating sections (30 μm for acute in vivo studies or 50 μm for hypothalamic sections) were processed as follows: 1) 3% normal goat serum (Vector Laboratories Z1104) for 2 hours to reduce nonspecific binding; 2) incubation with polyclonal anti-p-Erk1/2 antibody for 1 hour, RT (slice culture,

24 h; 4°C); 3) biotinylated secondary antibody for 1 hour, RT; 4) Avidin/Biotin Complex kit, per manufacturer's instructions (ABC Elite kit; Vector Laboratories); and 5) developed signal with 3, 3'-diaminobenzidine substrate (Vector Laboratories). Slides were then mounted, dehydrated through ethanol and cleared with xylene, and staining analyzed.

p-Erk 1/2 assessment

Assessment of p-Erk immunoreactive neurons was obtained by counting the number of p-Erk immuno-positive cells. Neurons with black or dark brown staining were considered as p-Erk positive. Coronal sections were counted for p-Erk immuno-positive staining bilaterally in PVH using a Zeiss Axio Imager A1 Microscope. Anatomic correlations were made according to landmarks given in Paxinos and Watson's stereotaxic atlas (bregma −0.58 to −1.22 mm were selected for PVH analysis) (33). The investigator counting the number of p-Erk immuno-positive cells was blinded to treatments received by the animals. Cell counts were taken over 2 consecutive central PVH sections from each experimental animal. The average number of p-Erk immuno-positive neurons per section for the brain nuclei mentioned above was calculated for 6 mice per experimental group. P-Erk data are expressed as mean ± SEM and analyzed by a Student's t test, with $P < .05$ considered significant.

NE turnover (NETO)

NETO was determined using the α-methyl-p-tyrosine (AMPT) method (34). Adult male mice were first adapted to handling and ip injections for 12 days before the actual experimental procedure to minimize handling- and injection-induced increases in SNS activity (35). Each animal was lightly restrained by hand, simulating the handling and injecting procedure. After habituation, the mice were infused with FGF21 or vehicle administered centrally via icv miniosmotic pump (methods above). After 5 days of infusion, we used the next method (36): food was removed at zeitgeber time (ZT)2 (ZTn is hours after light onset). At ZT4, one half of the vehicle-treated and one half of the FGF21-treated mice were killed by decapitation and adipose depots harvested for baseline NE content, whereas the other half were injected ip with 250-mg AMPT/kg body mass to inhibit tyrosine hydroxylase (36), the rate-limiting enzyme in catecholamine biosynthesis. AMPT (Sigma-Aldrich) was prepared in glacial acetic acid (1-μL/mg AMPT) and diluted to a final concentration in 0.15M NaCl. Upon AMPT administration, tissue levels of endogenous NE decline at a rate proportional to NE concentrations. To maintain tyrosine hydroxylase inhibition, at ZT6, these later mice were injected with a second lower ip dose

of AMPT (125-mg/kg body mass). The injected mice were killed at ZT8 by decapitation. Adipose depots harvested included IWAT, retroperitoneal WAT, epididymal WAT (EWAT), and interscapular BAT (IBAT), which were rapidly removed, weighed, and frozen in liquid nitrogen. NE adipose tissue content was measured using reverse-phase HPLC with electrochemical detection with some modifications (37) of Mefford's method (38). NETO was calculated according to the formula outlined in Vaughan et al (36).

Stromal-vascular fraction (SVF) culture and white adipocyte differentiation

IWAT from 10-week-old male β-less mice was dissected, washed, minced, and digested for 30–45 minutes at 37°C in PBS containing 10mM $CaCl_2$ and 200-U/mL collagenase type 1 (Worthington). Digested tissue was then filtered through a 100-μm cell strainer to remove undigested tissues. The flow-through was centrifuged at 600g for 5 minutes to pellet the SVF cells. The SVF cells were resuspended in a complete SVF culture medium (Dulbecco's Modified Eagle Medium F12; Life Technologies) containing an antibiotic-antimycotic (Life Technologies), and 10% fetal bovine serum, before filtering through a 70-μm cell strainer to remove clumps. After centrifugation as above, SVF cells were resuspended in SVF medium and transferred to tissue culture plates. When the SVF cells grew to confluence, adipocyte differentiation was performed as follows. At confluence (d 0) cells were exposed to an adipogeneic cocktail containing 5-μg/mL insulin and 1μM dexamethasone, 0.5mM isobutylmethylxanthine, and 1μM rosiglitazone in the SVF culture medium. Forty-eight hours after induction, cells were maintained in SVF culture medium containing 5-μg/mL insulin. At day 7 of differentiation, cells were treated for 24 hours with 100nM hFGF21 or 10μM forskolin (Sigma) in the absence of insulin and harvested at day 8.

Statistical analysis

Data are given as mean ± SEM. Statistical analysis was performed using a Student's t test or repeat measures ANOVA where appropriate. All statistical analyses were performed using GraphPad Prism 5 software and the differences were considered significant when $P < .05$.

Results

FGF21 stimulates p-Erk in the PVH in vivo and in vitro

To examine the ability of peripheral FGF21 to cross the blood brain barrier and signal in the central nervous system (CNS), we administered an ip injection of 24-μg FGF21; this is a similar dose to what we and others have used previously for acute signaling (39, 40). Thirty minutes after FGF21 injection, the mice were euthanized, and coronal brain sections were immunostained for p-ERK, a direct downstream target for FGF21 signaling (11). We found a strong signal in the PVH of FGF21-treated mice,

which was, on average, 2-fold higher than that seen in saline-treated mice ($P < .05$) (Figure 1, A–E).

To confirm that the FGF21 effect on the brain is direct and not due to a secondary signal from the periphery, we examined the effects of FGF21 on acutely harvested hypothalamic slices in vitro. Treatment with 100nM FGF21 increased p-Erk immunoreactivity in the PVH (Figure 1F, right) compared with vehicle control (Figure 1F, left).

These data indicated that FGF21 targets a specific region of the hypothalamus. We thus tested the hypothesis that FGF21 acts in the brain to mediate its peripheral effects by administering a low dose of FGF21 into the lateral ventricle.

Defining a dose for central infusion of FGF21

We first determined a dose that allowed us to isolate effects mediated by FGF21 signaling in the brain vs those mediated by the periphery in mice. Based on a previous report in rats (29), we used a dose of 0.4-μg/d icv of human FGF21, which was reported not to leak into the periphery. However, because diffusion properties could be different due to the size/weight of our mice, we then measured serum levels of hFGF21 and found that, in mice, there was a low, but detectable, level of hFGF21 in circulation of 246 ± 51 pg/mL above the ad libitum-fed level of 138 ± 20-pg/mL mouse FGF21. To ensure that this concentration in the serum did not have metabolic effects mediated through direct action on peripheral tissues, we tested several doses of peripheral FGF21 to attain the same serum level. We found that a sc dose of 1.6 μg/d achieved a serum concentration of (220 ± 45 pg/mL), which match that obtained by 0.4 μg/d administered centrally. None of the doses of FGF21 administered either icv or sc led to a significant change in body weight as shown in Supplemental Table 1 and in general weight change was less than 1 g.

Central FGF21 increases energy expenditure

We next examined the effect of central FGF21 on energy expenditure. At a dose of 0.4-μg/d icv-FGF21 increased metabolic rate (O_2 consumption) by 16% over 24 hours, which was largely due to a 17% increase in night cycle O_2 consumption (Figure 2A). We observed no changes in food intake (Figure 2B) or home cage activity (Figure 2C). Administration of peripheral FGF21 at 1.6 μg/d, which achieved the same serum level as the central 0.4-μg/d dose, had no effect on O_2 consumption (Figure 2D). This suggests that centrally administered FGF21 acts via the brain and not through the periphery. As systemic metabolic effects of FGF21 include changing metabolite levels, including lowering of circulating glucose and trig-

Figure 1. FGF21 induces Erk phosphorylation and increases sympathetic activity. Mice were injected ip with vehicle (n = 6) or FGF21 (n = 6). Representative images of PVH-containing coronal brain sections immunohistochemically labeled for p-Erk are shown (A) vehicle and (B) FGF21. Boxed regions are enlarged below each respective image (C and D). Mean number of p-Erk-positive cell counts taken over 2 consecutive central PVH sections for each experimental animal (E). Hypothalamic slice culture showed p-Erk in the PVH of FGF21-treated (right) but not vehicle-treated (left) (F). *, $P < .05$ by Student's t test.

β-hydroxybutyrate, glucose, and triglycerides did not change.

Central FGF21 increases "browning" markers in IWAT

Central FGF21 increased markers of IWAT browning, including 4-fold induction of *Ucp1* mRNA and 3-fold induction of deiodinase 2 (*Dio2*) mRNA (Figure 3A). There also was an increase in gene expression of factors involved in transcriptional regulation of adipogenesis, including *Pgc-1α* and *CCAAT/enhancer-binding protein (C/ebp)β*. Increased gene expression of mitochondrial associated markers, *cytochrome c oxidase polypeptide (Cox)7a* and *Cox8b* and genes involved in fatty acid oxidation, including *long-chain acyl-CoA dehydrogenase (Lcad)* and *very-Lcad (Vlcad)*, were all up-regulated in centrally treated mice. Interestingly, icv-FGF21 administration elevated *Fgf21* transcript in adipocytes, an effect which was not seen with high-dose sc infusion. The control dose of FGF21 of 1.6 μg/d sc had no effect on *Ucp1* and *Dio2* expression, indicating that the effects of 0.4 μg/d icv are centrally mediated (Figure 3B). Histologic examinations of IWAT from icv-FGF21 animals revealed morphologic changes associated with browning, including the appearance of Ucp1-enriched multilocular adipocytes (Figures 3, C–F).

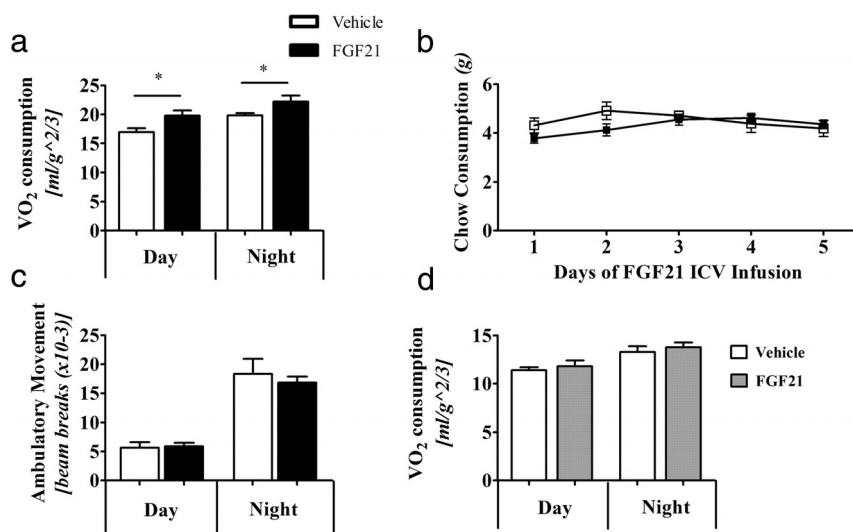## Central FGF21 activates IBAT and increases NETO in multiple adipose depots

Fgf21 expression increased in BAT with cold exposure and activation of this tissue may contribute to thermogenesis seen with central FGF21. Thus we looked for evidence of BAT activation by examining protein expression via Western blotting. We found a 40% increase in Ucp1 level upon icv-FGF21 administration (Figure 3G). We examined IBAT *Ucp1* gene expression and found these levels unchanged (data not shown); this is unsurprising,

lycerides, we next examined serum nutrient profiles of, glucose, triglycerides, and β-hydroxybutyrate in mice treated with icv-FGF21, or administered with FGF21 in the periphery (Table 1). Regardless of FGF21 delivery,

Figure 2. A low central FGF21 dose of 0.4 μg/d into WT mice causes an increase in O_2 consumption. Mice (n = 8 per group) administered icv-FGF21 have a higher metabolic rate of VO_2 (A), yet do not consume more food (vehicle, n = 8, FGF21, n = 7) (B) or have increased activity ambulatory activity (n = 14 per group) (C). Mice given the circulation-matching, 1.6-μg/d sc-FGF21 dose (vehicle, n = 6, FGF21 n = 8) do not show an increase in VO_2 consumption (D). Graphs are shown $\pm$ SEM. *, $P < .05$; **, $P < .01$; by Student's t test, food consumption not significant by repeat measures ANOVA, $P = .3193$.

because *Ucp1* mRNA in IBAT does not always reflect relative Ucp1 protein levels (41).

The central effects of FGF21 to activate the PVH may increase sympathetic action and this may mediate the browning of IWAT and increased Ucp1 in BAT (42, 43). Finally to confirm sympathetic activation directly we looked at NETO in target tissue depots, including IWAT, EWAT, and IBAT (Figure 3H). We observed an increase in IWAT NETO, a tissue known to brown, but minimal changes in EWAT NETO, which typically does not brown (Figure 3H). Interestingly, IBAT had the largest increase in NETO in response to central FGF21, which is in agreement with BAT activation by the SNS (for review see Ref. 44).

Adrenergic receptor blockade prevents the actions of central FGF21

Our aggregate data that FGF21 targets the PVH, browns IWAT, increases IWAT and IBAT NETO to activate BAT, all implicate SNS action (44). We thus predicted that adrenergic receptor blockade (ie, β-adrenoceptor antagonism) would inhibit the effects of icv-FGF21. Propranolol, a nonselective β-blocker, inhibited icv-FGF21 (0.4 μg/d) mediated induction of genes in IWAT (Figure 4A), including the induction of *Fgf21*. This blockade is specific to central FGF21 administration. By contrast, propranolol did not inhibit the induction of gene expression in IWAT in response to the standard peripheral pharmacological dose of FGF21 (24 μg/d). Thus, robust induction of *Ucp1* and *Lcad*, and increases in the mito-

chondrial genes *Cox7a* and *Cox8b*, persisted, despite propranolol treatment. Notably, the induction of *Ucp1* was more than 17-fold (Figure 4B), suggesting that when FGF21 is administered peripherally at high doses propranolol has little influence on direct FGF21 effects on the adipocyte. This is consistent with cell-autonomous effects of FGF21 on the adipocyte that we have previously reported (13).

To further explore the interaction between FGF21 and sympathetic activation, we used a genetic model of β-adrenoceptor ablation, the "β-less" mouse, which lacks all 3 β-adrenoceptors (30). In this mouse the end organ response to sympathetic activation is not possible. We found that icv-FGF21 treatment (0.4 μg/d) in β-less mice failed to produce changes in markers of thermogenesis, BAT-specific markers, or fatty acid oxidation (Figure 4C). Thus, in these mice, icv-FGF21 cannot induce the browning program in IWAT. These mice were also resistant to browning upon treatment with a standard peripheral dose of 24 μg/d of FGF21 infused over 5 days (Figure 4D). We also examined FGF21 receptor expression in adipose tissue of β-less mice. We found no significant differences in β-klotho and *Fgfr1* gene expression in IWAT. In BAT we found a 61% decrease in β-klotho ($P < .01$) and 29% decrease in *Fgfr1* ($P < .01$) in gene expression, compared with WT controls.

Because our previous work demonstrated a primary cell-autonomous effect of FGF21 on adipocytes (13), we wanted to further understand the lack of the cell-autonomous effect. We thus established primary adipocyte cultures from β-less mice. FGF21 is unable to elicit a direct response in β-less adipocytes (Figure 4D). These cells were still able to respond to forskolin, an activator of adenylyl cyclase downstream of adrenergic receptors (Figure 4E). These data suggest that the cell-autonomous effect of FGF21 is dependent on some degree of baseline activity of β-adrenergic receptor-linked signaling.

Discussion

FGF21 exerts multiple complex actions on metabolism. Along with direct effects on fatty acid oxidation in the liver and on glucose homeostasis in adipocytes, it plays a significant role in the systemic response to cold, including
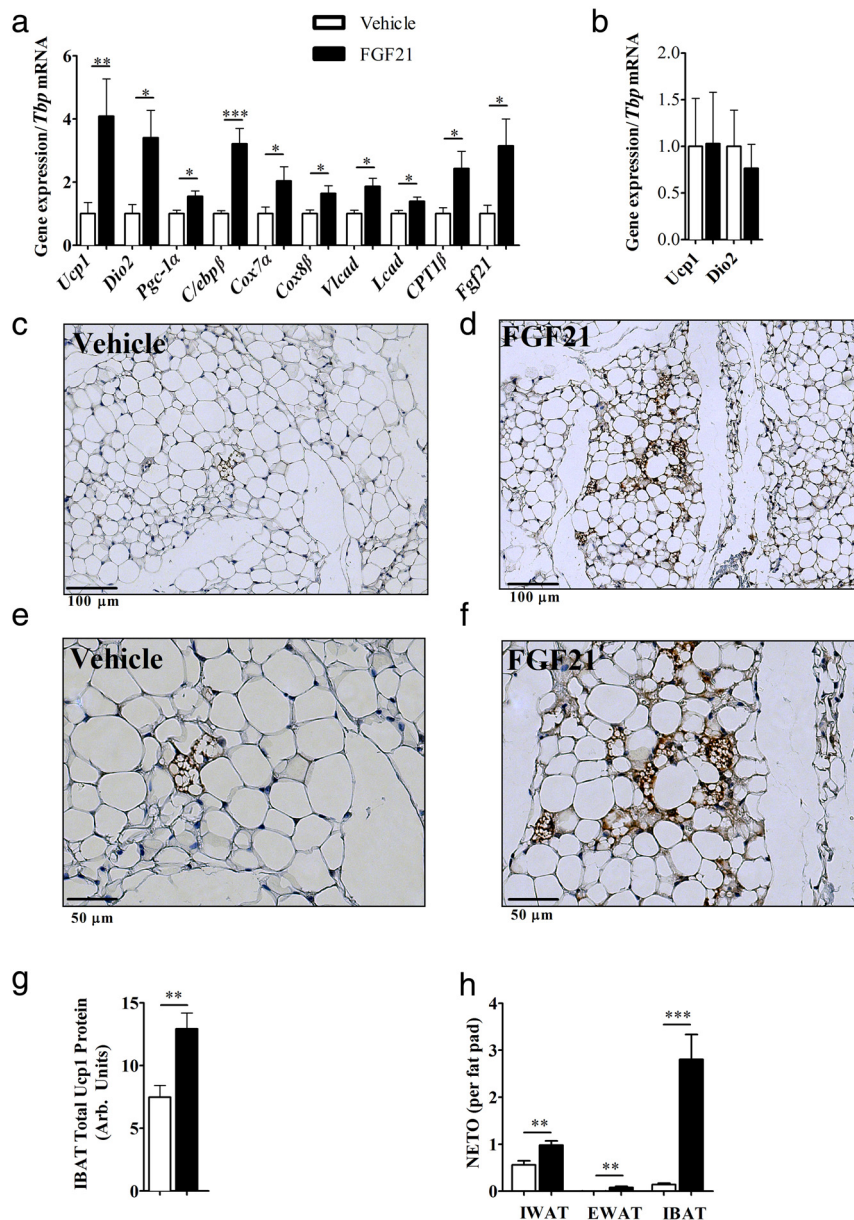
Figure 3. Browning profile of inguinal adipose tissue, Ucp1 protein expression in BAT, and NETO in adipose depots: icv-FGF21 (0.4 μg/d) 5-day infusion into mice (n = 15 per group) causes increases in expression of BAT-specific markers and markers of thermogenesis and fatty acid oxidation in IWAT (A), whereas a circulation-matching sc-FGF21 dose (1.6 μg/d) (n = 7 per group) fails to induce expression of *Ucp1* or *Dio2* after 5 days of treatment (B). Histologic examinations (vehicle, n = 8, FGF21, n = 7) of IWAT revealed that 5-day icv-FGF21 administration (0.4 μg/d) caused increased protein expression of Ucp1 as assessed immunohistochemistry (C–F). IBAT total Ucp1 protein is increased after 5-day icv-FGF21 (0.4 μg/d)-treated mice (vehicle, n = 7, FGF21, n = 6) (G). NETO increased after a 5-day icv-FGF21 administration in IWAT (vehicle, n = 16, FGF21 n = 19), EWAT (vehicle n = 16, FGF21, n = 20), and IBAT (vehicle, n = 17, FGF21, n = 20) (H). *Carnitine palmitoyltransferase 1b* (*Cpt1β*). Graphs are shown as mean $\pm$ SEM. *, $P < .05$; **, $P < .01$; ***, $P > .001$ by Student's *t* test.

ergy expenditure, was possible even after surgical removal of the main interscapular brown fat pad (15) demonstrating the relevance of adipose depots outside IBAT. The data presented here show, for the first time, that FGF21 acts in the brain to activate the SNS to induce browning of WAT depots and stimulate thermogenesis-associated protein expression in BAT. Although FGF21 does not appear to be expressed in the brain (27), it crosses the blood brain barrier in mice (23). Thus, FGF21 central action would be analogous to that of other peptides synthesized in the periphery, and act on the brain to control energy balance, appetite and glucose homeostasis, including leptin (45), ghrelin (46), glucagon-like peptide-1 (47), and insulin (48). Consistent with this central action are recent reports demonstrating that icv-FGF21 infusions control insulin sensitivity (29). In addition, mice overexpressing FGF21 have impaired fertility and circadian rhythms due to effects on the suprachiasmatic nucleus (25, 26).

This effect of central FGF21 to increase sympathetic activity is likely mediated through the PVH, which is consistent with the known role of this nucleus to integrate sympathetic outflow. However, it does not rule out other periventricular hypothalamic sites and possibly, due to the direction of CSF flow, other sites involved in the SNS outflow from brain to adipose tissues (42). The finding that central FGF21 increased NETO in multiple adipose depots is a direct demonstration of increased sympathetic outflow to these tissues. The resulting elevated NE signaling leads to amplified browning of IWAT as demonstrated by changes in gene expression and morphology and activation of IBAT as demonstrated by a boost in Ucp1 protein levels, all of which likely increases O_2 consumption. Although the role of WAT in thermogenesis is debated (49), thermogenically active WAT now appears to be an important contributor to metabolic rate
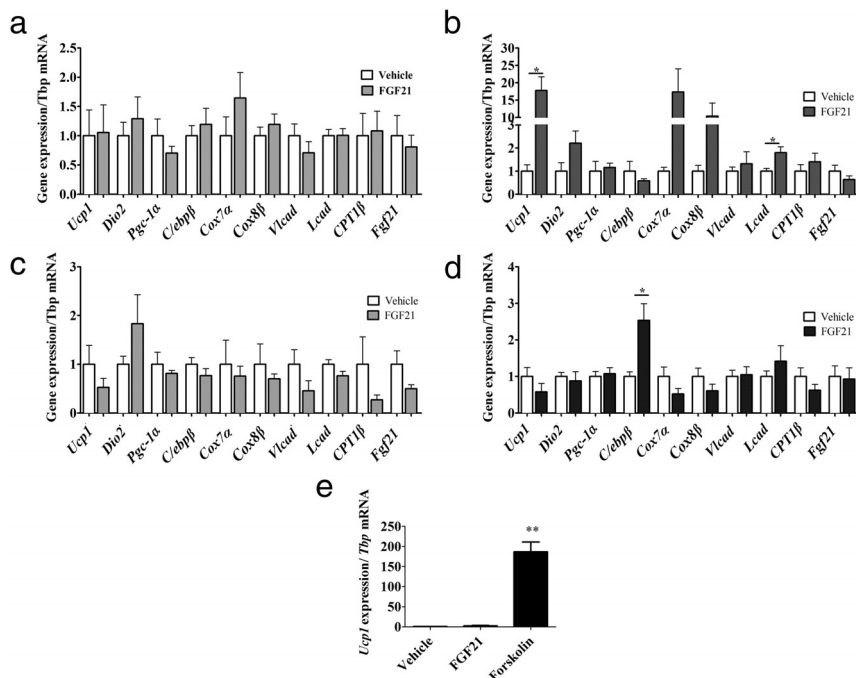
browning of WAT (13) and thermogenic adaptation of BAT (14, 21). Although the significance of BAT to thermogenic adaptation must not be underestimated, the relative contribution of browning of WAT is increasingly seen as an important and significant depot. Indeed, recent work showed that FGF21 action, including increased en-

Figure 4. Central FGF21 is dependent on the SNS. The β-blocker propranolol counters the influence of FGF21 on IWAT and β-adrenoceptors are required for FGF21-mediated induction of BAT-specific markers, thermogenesis, and fatty acid oxidation in IWAT. IWAT of 5-day icv administration (0.4 μg/d) of FGF21 fails to induce gene expression of a panel of markers of browning in IWAT if the mice (n = 7 per group) are treated with the general β-blocker propranolol (A), but this is largely overcome if administered a large sc-FGF21 dose (24 μg/d) (vehicle, n = 6, FGF21 n = 8) plus propranolol (B). Mice lacking the β1, β2, and β3 adrenoceptors (β-less mice) fail to induce a browning profile in IWAT if given FGF21 (0.4 μg/d) icv (vehicle, n = 9, FGF21, n = 8) (C) or if administered a large sc-FGF21 dose (24 μg/d) to β-less mice (vehicle, n = 7, FGF21, n = 6) (D). Primary IWAT culture derived from β-less mice was unresponsive to vehicle or FGF21 treatment but did induce *Ucp1* when treated with forskolin (E). Graphs are shown as mean ± SEM. *, $P < .05$; **, $P < .01$ by Student's *t* test.

and several groups have shown that genetic manipulations that lead to browning of WAT can increase energy expenditure and cause weight loss. Examples of this include both gain-of-function mice (Ucp1, PR domain containing 16 and loss-of-function mouse models (aldehyde dehydrogenase 1 family, member A1, cell death-inducing DNA fragmentation factor A-like effector C, eukaryotic translation initiation factor 4e-binding protein 1, nuclear receptor-interacting protein 1, mothers against decapentaplegic homolog 3, and vascular endothelial growth factor A (50–60). In addition, in the only demonstration of heat generation by browned WAT, neuropeptide Y knockdown specifically in the dorsomedial hypothalamic nucleus increases browned IWAT temperature in vivo (61), an effect also mediated by the SNS drive to this tissue (62).

There appear to be 2 distinct pathways for FGF21-induced browning and activation of IBAT (Figure 5): one pathway that directly acts on the adipocyte in a cell autonomous manner that we previously described (13) and a second pathway that acts via the brain and the SNS to simulate browning of WAT and activation of BAT. Before

the present study, effects of FGF21 on both of these tissues were understood to be direct (13, 14, 21). We demonstrated the direct cell-autonomous stabilization of Pgc-1α in IWAT (13). Most of these studies, however, used peripheral FGF21 administered at high doses and did not account for FGF21 crossing the blood brain barrier, and therefore did not address the possibility of a central action. Based on our results wherein central administration of FGF21 leads to a "brown/brite" IWAT depot, we developed a working model wherein FGF21 acts in the brain, most likely through the hypothalamus but possibly through other areas of the neuroaxis such as the hindbrain (for review see Ref. 44) to relay signals to the IML and then sympathetic ganglia before ultimately innervating IWAT to promote browning (Figure 5). In addition, in IWAT, sympathetic activation is associated with an increase in locally produced FGF21 suggesting that central FGF21 "feeds forward" to generate Fgf21 that can act locally in a cell-autonomous fashion.

These results define a second pathway for FGF21 action mediated through the CNS, which we identify by low-dose FGF21 infusion into the brain. Are there perturbations that lead to increases of peripheral Fgf21 that can cross the blood brain barrier and act centrally? One such circumstance is consumption of a KD, which induces a 25-fold increase in hepatic *Fgf21* expression and markedly elevates Fgf21 in the serum to what might otherwise be considered pharmacological levels. Indeed, mice consuming KD show evidence of sympathetic activation as assessed by marked increases in O_2 consumption and a 5-fold increase in BAT Ucp1 protein levels (63). Critically, the thermogenic effects of KD are absent in Fgf21-deficient mice (64). These central actions likely reflect the emerging dual actions of this peptide as both a paracrine and endocrine regulator of thermogenesis.

The data here are consistent with a recent report examining CNS deletion of *β-klotho*, which also concluded that FGF21 acts through the CNS to increase sympathetic activity (65), which was assessed using indirect electrophysiologic data of both sensory and SNS
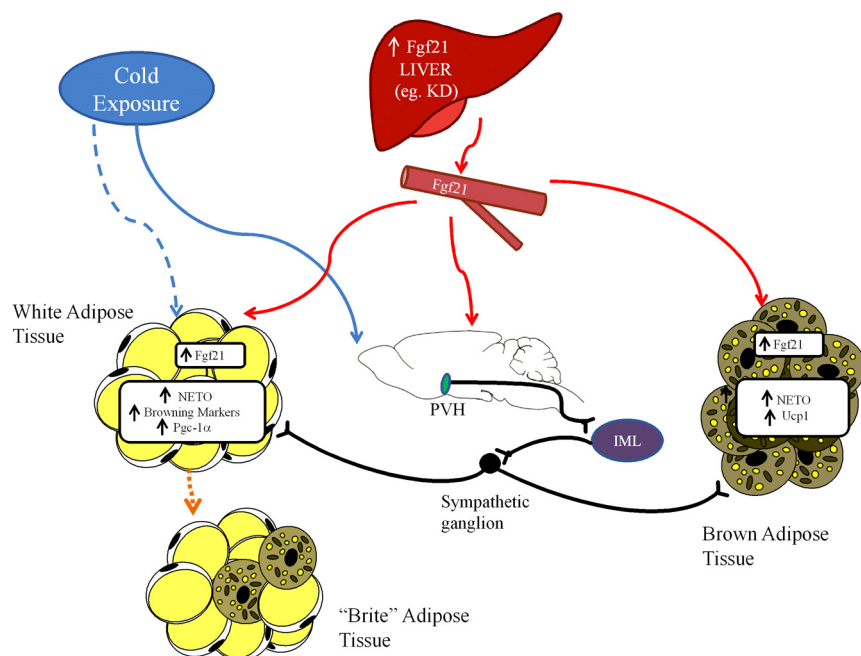
Figure 5. Physiologic model of FGF21 action. Fgf21 is increased systemically via increased production in the liver, such as through consumption of a KD. This Fgf21 can act directly on adipose tissue, including WAT where it can induce browning. Fgf21 can also cross the blood-brain barrier and act on the PVH, which activates a cholinergic signal from the IML to increase β-adrenergic signaling in sympathetic ganglia to increase adrenergic activity in target thermogenic tissues such as BAT and WAT. When animals are exposed to cold, SNS activation occurs via pathways independent of central or peripheral FGF21. Increased β-adrenergic signaling in target tissue induces *Fgf21* expression in WAT and BAT. In this later case, Fgf21 acts as a local autocrine/paracrine factor to drive thermogenesis.

blocked the central effects of FGF21. By contrast, as expected, propranolol only attenuated the effects of sc-administered FGF21, because in the periphery, FGF21 can also act autonomously on the adipocyte.

Intriguingly, mice lacking all 3 β-adrenoceptors through genetic ablation failed to respond to either central or peripheral FGF21. The lack of responsiveness could be at least partially due to lower expression of Fgf21 receptors in the BAT of β-less mice; reductions in β-*klotho* expression in adipose tissue have been reported and may account for impaired FGF21 responsiveness (5, 9, 10, 68, 69). Furthermore, the β-less mouse's lack of response to central FGF21 is consistent with the requirement for activation of SNS-mediated adrenoceptor signaling. The fact that the β-less mice fail to respond to peripheral FGF21 when one would expect direct, cell-autonomous FGF21-mediated browning is unexpected. We explored this further with primary cultures and found that FGF21 fails to induce *Ucp1* in primary β-less WAT, an effect that is readily seen in WT culture. However, WAT of β-less mice, can brown under special circumstances. Although they fail to respond to acute to cold, they will eventually brown with long-term exposure (30, 70). Furthermore the β-less primary cells respond to forskolin, which bypasses adrenoceptors and acts directly to increase intracellular cyclic adenosine monophosphate, ultimately increasing *Ucp1* expression. These results from the β-less models indicate a baseline requirement of adrenoceptor activity for appropriate browning whether induced by cold exposure or FGF21.

Taken together, these studies demonstrate that FGF21 can regulate sympathetic activity through direct action in the brain and that this pathway contributes to adaptive thermogenesis by the hormone. In addition, we demonstrated that the PVH and/or other periventricular sites downstream from the third ventricle is a target for FGF21 action. Future studies should address the relative contribution of peripheral vs central action in mediating the broader array of FGF21 metabolic effects and also to better understand the physiologic interaction of FGF21 and the SNS. Finally, site-specific FGF21 injection into neurons known to possess Fgf21 receptors in the hypothalamus, midbrain and hindbrain can pinpoint the structure(s)

nerves innervating BAT after an icv-FGF21 injection and focused on the role of FGF21 in mediating classical BAT thermogenesis.

Physiologic control of FGF21 expression is complex and differs between WAT and liver. It seems likely that serum levels reflect Fgf21 derived from the liver whether induced by fasting, KD, or fatty liver disease as these manipulations do not induce *Fgf21* expression in WAT. Adipose tissues do not appear to contribute to serum levels, as manipulations that increase expression in adipose, including cold exposure and Pparγ agonists are not associated with changes in the circulation (13, 66, 67). Thus, the central action is likely to be the consequence of conditions that significantly induce hepatic expression, particularly dietary manipulations (4, 63). Under these conditions, Fgf21 acting through the CNS will induce its own expression, creating a novel regulatory loop from the liver to the brain to adipose tissue linked by the SNS.

The PVH mediates sympathetic activity through a cascade of events. Direct PVH innervation of the IML increases cholinergic activity and activates downstream adrenergic outflow from sympathetic ganglia to increase NE release in target tissues. NE is thus a direct effector of end-organ tissue activation. When we used propranolol to block NE signaling through adrenoceptors, we completely

responsible for the ultimate SNS activational effects observed here.

References

1. **Inagaki T, Dutchak P, Zhao G, et al.** Endocrine regulation of the fasting response by PPARα-mediated induction of fibroblast growth factor 21. *Cell Metab*. 2007;5(6):415–425.
2. **Badman MK, Pissios P, Kennedy AR, Koukos G, Flier JS, Maratos-Flier E.** Hepatic fibroblast growth factor 21 is regulated by PPARα and is a key mediator of hepatic lipid metabolism in ketotic states. *Cell Metab*. 2007;5(6):426–437.
3. **Pissios P, Hong S, Kennedy AR, Prasad D, Liu FF, Maratos-Flier E.** Methionine and choline regulate the metabolic phenotype of a ketogenic diet. *Mol Metab*. 2013;2(3):306–313.
4. **De Sousa-Coelho AL, Marrero PF, Haro D.** Activating transcription factor 4-dependent induction of FGF21 during amino acid deprivation. *Biochem J*. 2012;443(1):165–171.
5. **Ogawa Y, Kurosu H, Yamamoto M, et al.** βKlotho is required for metabolic activity of fibroblast growth factor 21. *Proc Natl Acad Sci USA*. 2007;104(18):7432–7437.
6. **Kharitonenkov A, Dunbar JD, Bina HA, et al.** FGF-21/FGF-21 receptor interaction and activation is determined by βKlotho. *J Cell Physiol*. 2008;215(1):1–7.
7. **Suzuki M, Uehara Y, Motomura-Matsuzaka K, et al.** βKlotho is required for fibroblast growth factor (FGF) 21 signaling through FGF receptor (FGFR) 1c and FGFR3c. *Mol Endocrinol*. 2008;22(4):1006–1014.
8. **Yang C, Jin C, Li X, Wang F, McKeehan WL, Luo Y.** Differential specificity of endocrine FGF19 and FGF21 to FGFR1 and FGFR4 in complex with KLB. *PLoS One*. 2012;7(3):e33870.
9. **Adams AC, Cheng CC, Coskun T, Kharitonenkov A.** FGF21 requires βklotho to act in vivo. *PLoS One*. 2012;7(11):e49977.
10. **Ding X, Boney-Montoya J, Owen BM, et al.** βKlotho is required for fibroblast growth factor 21 effects on growth and metabolism. *Cell Metab*. 2012;16(3):387–393.
11. **Kharitonenkov A, Shiyanova TL, Koester A, et al.** FGF-21 as a novel metabolic regulator. *J Clin Invest*. 2005;115(6):1627–1635.
12. **Coskun T, Bina HA, Schneider MA, et al.** Fibroblast growth factor 21 corrects obesity in mice. *Endocrinology*. 2008;149(12):6018–6027.
13. **Fisher FM, Kleiner S, Douris N, et al.** FGF21 regulates PGC-1α and browning of white adipose tissues in adaptive thermogenesis. *Genes Dev*. 2012;26(3):271–281.
14. **Hondares E, Iglesias R, Giralt A, et al.** Thermogenic activation induces FGF21 expression and release in brown adipose tissue. *J Biol Chem*. 2011;286(15):12983–12990.
15. **Emanuelli B, Vienberg SG, Smyth G, et al.** Interplay between FGF21 and insulin action in the liver regulates metabolism. *J Clin Invest*. 2014;124(2):515–527.
16. **Lee P, Brychta RJ, Linderman J, Smith S, Chen KY, Celi FS.** Mild cold exposure modulates fibroblast growth factor 21 (FGF21) diurnal rhythm in humans: relationship between FGF21 levels, lipolysis, and cold-induced thermogenesis. *J Clin Endocrinol Metab*. 2012;98(1):102.
17. **Shabalina IG, Petrovic N, de Jong JM, Kalinovich AV, Cannon B, Nedergaard J.** UCP1 in brite/beige adipose tissue mitochondria is functionally thermogenic. *Cell Rep*. 2013;5(5):1196–1203.
18. **Harms M, Seale P.** Brown and beige fat: development, function and therapeutic potential. *Nat Med*. 2013;19(10):1252–1263.
19. **Bonet ML, Oliver P, Palou A.** Pharmacological and nutritional agents promoting browning of white adipose tissue. *Biochim Biophys Acta*. 2013;1831(5):969–985.
20. **Hondares E, Rosell M, Gonzalez FJ, Giralt M, Iglesias R, Villarroya F.** Hepatic FGF21 expression is induced at birth via PPARα in response to milk intake and contributes to thermogenic activation of neonatal brown fat. *Cell Metab*. 2010;11(3):206–212.
21. **Chartoumpekis DV, Habeos IG, Ziros PG, Psyrogiannis AI, Kyriazopoulou VE, Papavassiliou AG.** Brown adipose tissue responds to cold and adrenergic stimulation by induction of FGF21. *Mol Med*. 2011;17(7–8):736–740.
22. **Bamshad M, Aoki VT, Adkison MG, Warren WS, Bartness TJ.** Central nervous system origins of the sympathetic nervous system outflow to white adipose tissue. *Am J Physiol*. 1998;275(1 pt 2):R291–R299.
23. **Hsuchou H, Pan W, Kastin AJ.** The fasting polypeptide FGF21 can enter brain from blood. *Peptides*. 2007;28(12):2382–2386.
24. **Tan BK, Hallschmid M, Adya R, Kern W, Lehnert H, Randeva HS.** Fibroblast growth factor 21 (FGF21) in human cerebrospinal fluid: relationship with plasma FGF21 and body adiposity. *Diabetes*. 2011;60(11):2758–2762.
25. **Bookout AL, de Groot MH, Owen BM, et al.** FGF21 regulates metabolism and circadian behavior by acting on the nervous system. *Nat Med*. 2013;19(9):1147–1152.
26. **Owen BM, Bookout AL, Ding X, et al.** FGF21 contributes to neuroendocrine control of female reproduction. *Nat Med*. 2013;19(9):1153–1156.
27. **Fon Tacer K, Bookout AL, Ding X, et al.** Research resource: comprehensive expression atlas of the fibroblast growth factor system in adult mouse. *Mol Endocrinol*. 2010;24(10):2050–2064.
28. **Yazaki N, Fujita H, Ohta M, Kawasaki T, Itoh N.** The structure and expression of the FGF receptor-1 mRNA isoforms in rat tissues. *Biochim Biophys Acta*. 1993;1172(1–2):37–42.
29. **Sarruf DA, Thaler JP, Morton GJ, et al.** Fibroblast growth factor 21 action in the brain increases energy expenditure and insulin sensitivity in obese rats. *Diabetes*. 2010;59(7):1817–1824.
30. **Bachman ES, Dhillon H, Zhang CY, et al.** βAR signaling required for diet-induced thermogenesis and obesity resistance. *Science*. 2002;297(5582):843–845.
31. **Khan AM, Ponzio TA, Sanchez-Watts G, Stanley BG, Hatton GI, Watts AG.** Catecholaminergic control of mitogen-activated protein kinase signaling in paraventricular neuroendocrine neurons in vivo and in vitro: a proposed role during glycemic challenges. *J Neurosci*. 2007;27(27):7344–7360.
32. **Chee MJ, Myers MG Jr, Price CJ, Colmers WF.** Neuropeptide Y suppresses anorexigenic output from the ventromedial nucleus of the hypothalamus. *J Neurosci*. 2010;30(9):3380–3390.
33. **Paxinos G, Franklin KBJ.** *The Mouse Brain in Stereotaxic Coordinates.* vol 3, 2nd ed. Boston, MA: Academic Press; 2001.

34. **Spector S, Sjoerdsma A, Udenfriend S.** Blockade of endogenous nor-epinephrine synthesis by α-methyl-tyrosine, an inhibitor of tyrosine hyxroxylase. *J Pharmacol Exp Ther*. 1965;147:86–95.

35. **Shrestha YB, Vaughan CH, Smith BJ Jr, Song CK, Baro DJ, Bartness TJ.** Central melanocortin stimulation increases phosphorylated per-ilipin A and hormone-sensitive lipase in adipose tissues. *Am J Physiol Regul Integr Comp Physiol*. 2010;299(1):R140–R149.

36. **Vaughan CH, Zarebidaki E, Ehlen JC, Bartness TJ.** Analysis and measurement of the sympathetic and sensory innervation of white and brown adipose tissue. *Methods Enzymol*. 2014;537:199–225.

37. **Youngstrom TG, Bartness TJ.** Catecholaminergic innervation of white adipose tissue in Siberian hamsters. *Am J Physiol*. 1995;268(3 pt 2):R744–R751.

38. **Mefford IN.** Application of high performance liquid chromatography with electrochemical detection to neurochemical analysis: mea-surement of catecholamines, serotonin and metabolites in rat brain. *J Neurosci Methods*. 1981;3(3):207–224.

39. **Potthoff MJ, Inagaki T, Satapati S, et al.** FGF21 induces PGC-1α and regulates carbohydrate and fatty acid metabolism during the adap-tive starvation response. *Proc Natl Acad Sci USA*. 2009;106(26): 10853–10858.

40. **Fisher FM, Estall JL, Adams AC, et al.** Integrated regulation of hepatic metabolism by fibroblast growth factor 21 (FGF21) in vivo. *Endocrinology*. 2011;152(8):2996–3004.

41. **Nedergaard J, Cannon B.** UCP1 mRNA does not produce heat. *Biochim Biophys Acta*. 2013;1831(5):943–949.

42. **Nguyen NL, Randall J, Banfield BW, Bartness TJ.** Central sympa-thetic innervations to visceral and subcutaneous white adipose tis-sue. *Am J Physiol Regul Integr Comp Physiol*. 2014;306(6):R375–R386.

43. **Romanovsky AA.** Thermoregulation: some concepts have changed. Functional architecture of the thermoregulatory system. *Am J Physiol Regul Integr Comp Physiol*. 2007;292(1):R37–R46.

44. **Bartness TJ, Vaughan CH, Song CK.** Sympathetic and sensory in-nervation of brown adipose tissue. *Int J Obes*. 2010;34(suppl 1): S36–S42.

45. **Ahima RS, Flier JS.** Leptin. *Annu Rev Physiol*. 2000;62:413–437.

46. **van der Lely AJ, Tschöp M, Heiman ML, Ghigo E.** Biological, phys-iological, pathophysiological, and pharmacological aspects of ghre-lin. *Endocr Rev*. 2004;25(3):426–457.

47. **Baggio LL, Drucker DJ.** Biology of incretins: GLP-1 and GIP. *Gas-troenterology*. 2007;132(6):2131–2157.

48. **Saltiel AR, Kahn CR.** Insulin signalling and the regulation of glucose and lipid metabolism. *Nature*. 2001;414(6865):799–806.

49. **Nedergaard J, Cannon B.** The browning of white adipose tissue: some burning issues. *Cell Metab*. 2014;20(3):396–407.

50. **Kopecky J, Clarke G, Enerbäck S, Spiegelman B, Kozak LP.** Expres-sion of the mitochondrial uncoupling protein gene from the aP2 gene promoter prevents genetic obesity. *J Clin Invest*. 1995;96(6):2914–2923.

51. **Stefl B, Janovská A, Hodný Z, et al.** Brown fat is essential for cold-induced thermogenesis but not for obesity resistance in aP2-Ucp mice. *Am J Physiol*. 1998;274(3 pt 1):33.

52. **Seale P, Conroe HM, Estall J, et al.** Prdm16 determines the thermo-genic program of subcutaneous white adipose tissue in mice. *J Clin Invest*. 2011;121(1):96–105.

53. **Kiefer FW, Vernochet C, O'Brien P, et al.** Retinaldehyde dehydro-genase 1 regulates a thermogenic program in white adipose tissue. *Nat Med*. 2012;18(6):918–925.

54. **Toh SY, Gong J, Du G, et al.** Up-regulation of mitochondrial activity and acquirement of brown adipose tissue-like property in the white adipose tissue of fsp27 deficient mice. *PLoS One*. 2008;3(8):e2890.

55. **Tsukiyama-Kohara K, Poulin F, Kohara M, et al.** Adipose tissue reduction in mice lacking the translational inhibitor 4E-BP1. *Nat Med*. 2001;7(10):1128–1132.

56. **Christian M, Kiskinis E, Debevec D, Leonardsson G, White R, Parker MG.** RIP140-targeted repression of gene expression in adi-pocytes. *Mol Cell Biol*. 2005;25(21):9383–9391.

57. **Leonardsson G, Steel JH, Christian M, et al.** Nuclear receptor core-pressor RIP140 regulates fat accumulation. *Proc Natl Acad Sci USA*. 2004;101(22):8437–8442.

58. **Powelka AM, Seth A, Virbasius JV, et al.** Suppression of oxidative metabolism and mitochondrial biogenesis by the transcriptional corepressor RIP140 in mouse adipocytes. *J Clin Invest*. 2006; 116(1):125–136.

59. **Yadav H, Quijano C, Kamaraju AK, et al.** Protection from obesity and diabetes by blockade of TGF-β/Smad3 signaling. *Cell Metab*. 2011;14(1):67–79.

60. **Lu X, Ji Y, Zhang L, et al.** Resistance to obesity by repression of VEGF gene expression through induction of brown-like adipocyte differentiation. *Endocrinology*. 2012;153(7):3123–3132.

61. **Bi S.** Dorsomedial hypothalamic NPY modulation of adiposity and thermogenesis. *Physiol Behav*. 2013;121:56–60.

62. **Chao PT, Yang L, Aja S, Moran TH, Bi S.** Knockdown of NPY expression in the dorsomedial hypothalamus promotes develop-ment of brown adipocytes and prevents diet-induced obesity. *Cell Metab*. 2011;13(5):573–583.

63. **Kennedy AR, Pissios P, Otu H, et al.** A high-fat, ketogenic diet induces a unique metabolic state in mice. *Am J Physiol Endocrinol Metab*. 2007;292(6):E1724–E1739.

64. **Badman MK, Koester A, Flier JS, Kharitonenkov A, Maratos-Flier E.** Fibroblast growth factor 21-deficient mice demonstrate impaired adaptation to ketosis. *Endocrinology*. 2009;150(11):4931–4940.

65. **Owen BM, Ding X, Morgan DA, et al.** FGF21 acts centrally to induce sympathetic nerve activity, energy expenditure, and weight loss. *Cell Metab*. 2014;20(4):670–677.

66. **Dutchak PA, Katafuchi T, Bookout AL, et al.** Fibroblast growth factor-21 regulates PPARγ activity and the antidiabetic actions of thiazolidinediones. *Cell*. 2012;148(3):556–567.

67. **Adams AC, Coskun T, Cheng CC, O Farrell LS, Dubois SL, Khari-tonenkov A.** Fibroblast growth factor 21 is not required for the antidiabetic actions of the thiazoladinediones. *Mol Metab*. 2013; 2(3):205–214.

68. **Díaz-Delfín J, Hondares E, Iglesias R, Giralt M, Caelles C, Villar-roya F.** TNF-α represses β-Klotho expression and impairs FGF21 action in adipose cells: involvement of JNK1 in the FGF21 pathway. *Endocrinology*. 2012;153(9):4238–4245.

69. **Fisher FM, Chui PC, Antonellis PJ, et al.** Obesity is a fibroblast growth factor 21 (FGF21)-resistant state. *Diabetes*. 2010;59(11): 2781–2789.

70. **Ye L, Wu J, Cohen P, et al.** Fat cells directly sense temperature to activate thermogenesis. *Proc Natl Acad Sci USA*. 2013;110(30): 12480–12485.